

MODELING THORACIC BLUNT TRAUMA; TOWARDS A FINITE-ELEMENT-BASED DESIGN METHODOLOGY FOR BODY ARMOR

Martin N. Raftenberg
U. S. Army Research Laboratory
Aberdeen Proving Ground, MD 21005-5069

ABSTRACT

ARL is pursuing the goal of developing a finite-element-based design methodology for thoracic body armor. We describe progress in modeling two essential ingredients, a Kevlar vest and the human thorax.

1. INTRODUCTION

Thoracic armor is generally designed by an experimental methodology, which, since the 1980s, has been based on the clay-backed test codified in an NIJ standard (National Institute of Justice, 1987). This test involves placing the armor on a standardized block of clay, shooting the armor with the “design threat,” and then measuring the depth of the crater left in the clay. No account is taken of hit location on the thorax, and as a result Kevlar vests are currently not tapered to save on weight. Nor is account taken of the time sequence of thoracic events as a response to the impact; only the permanent deformation in the clay is measured.

Since at least the early 1990s, the automotive industry has been engaged in the development of 3D finite element (FE) models of the human thorax for use in numerical crash simulations. In 1999 ARL explored the potential for transitioning to the field of body armor design these advances in FE thorax modeling. The Wayne State thorax model (WSTM) (Wang, 1995) was found to be the most anatomically detailed model available. Figure 1 shows that model’s representation of the skeletal, circulatory, and respiratory systems.

ARL purchased access to the WSTM in 2000 to use it as a starting point for the development of a new, simulation-based methodology for body armor design. Figure 2 shows an overview of our proposed approach. An FE model of a body armor design is placed on the thorax model, and the two are then impacted with a model of the threat. The three models each consist of an FE mesh (discretized geometry/anatomy) and a representation of all materials’ mechanical properties. The simulation is run on an FE code such as LS-DYNA (Livermore Software Technology Corp., 2003). The immediate output is local stresses and displacements throughout the thorax, which must then be related to quantitative injury assessment. The designer then systematically modifies the armor and observes the

resulting changes in the simulation results, thereby seeking an optimal design.

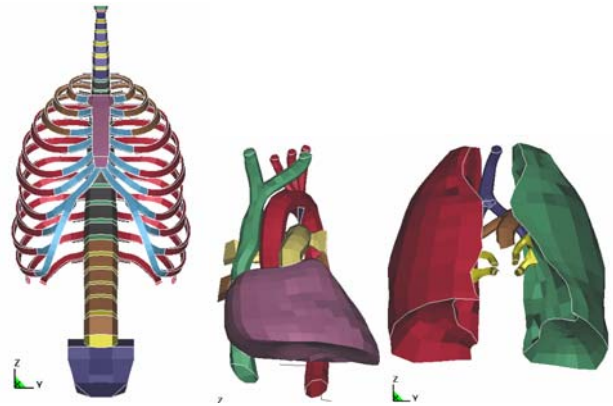


Fig.1. Skeletal, cardiovascular, and respiratory systems as represented in the Wayne State Thorax Model.

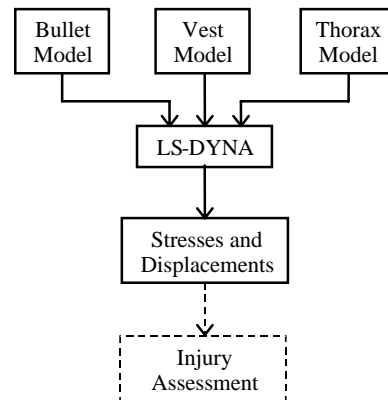


Fig. 2. Calculation overview.

In Section 2 the WSTM is applied to the case of the M882 bullet at 445 m/s versus a multi-ply Kevlar vest plus thorax. For this situation, accelerometer data from instrumented human thoracic tissue were available to serve as benchmarks for the simulations (Mackiewicz et al., in preparation).

Section 3 describes an orthotropic, nonlinearly elastic constitutive model for a Kevlar vest. Section 4 describes

Report Documentation Page				Form Approved OMB No. 0704-0188	
Public reporting burden for the collection of information is estimated to average 1 hour per response, including the time for reviewing instructions, searching existing data sources, gathering and maintaining the data needed, and completing and reviewing the collection of information. Send comments regarding this burden estimate or any other aspect of this collection of information, including suggestions for reducing this burden, to Washington Headquarters Services, Directorate for Information Operations and Reports, 1215 Jefferson Davis Highway, Suite 1204, Arlington VA 22202-4302. Respondents should be aware that notwithstanding any other provision of law, no person shall be subject to a penalty for failing to comply with a collection of information if it does not display a currently valid OMB control number.					
1. REPORT DATE 00 DEC 2004		2. REPORT TYPE N/A		3. DATES COVERED -	
4. TITLE AND SUBTITLE Modeling Thoracic Blunt Trauma; Towards A Finite-Element-Based Design Methodology For Body Armor				5a. CONTRACT NUMBER	
				5b. GRANT NUMBER	
				5c. PROGRAM ELEMENT NUMBER	
6. AUTHOR(S)				5d. PROJECT NUMBER	
				5e. TASK NUMBER	
				5f. WORK UNIT NUMBER	
7. PERFORMING ORGANIZATION NAME(S) AND ADDRESS(ES) U. S. Army Research Laboratory Aberdeen Proving Ground, MD 21005-5069				8. PERFORMING ORGANIZATION REPORT NUMBER	
9. SPONSORING/MONITORING AGENCY NAME(S) AND ADDRESS(ES)				10. SPONSOR/MONITOR'S ACRONYM(S)	
				11. SPONSOR/MONITOR'S REPORT NUMBER(S)	
12. DISTRIBUTION/AVAILABILITY STATEMENT Approved for public release, distribution unlimited					
13. SUPPLEMENTARY NOTES See also ADM001736, Proceedings for the Army Science Conference (24th) Held on 29 November - 2 December 2005 in Orlando, Florida. , The original document contains color images.					
14. ABSTRACT					
15. SUBJECT TERMS					
16. SECURITY CLASSIFICATION OF:			17. LIMITATION OF ABSTRACT UU	18. NUMBER OF PAGES 27	19a. NAME OF RESPONSIBLE PERSON
a. REPORT unclassified	b. ABSTRACT unclassified	c. THIS PAGE unclassified			

progress towards the development of a thorax FE model that is computationally more robust than the WSTM.

2. AN APPLICATION OF WSTM TO A BALLISTICS SIMULATION

NIJ Level 3A body armor is intended to offer protection against semiautomatic weapons and generally takes the form of a fabric vest. National Institute of Justice (1987) specifies the Level 3A “design threat” to be the M882 bullet impacting at a minimum velocity of 427 m/s. This bullet is a standard NATO round composed of a lead core and a copper gilding jacket. Its diameter is 9 mm, and its mass is 8 grams (Fig. 3).

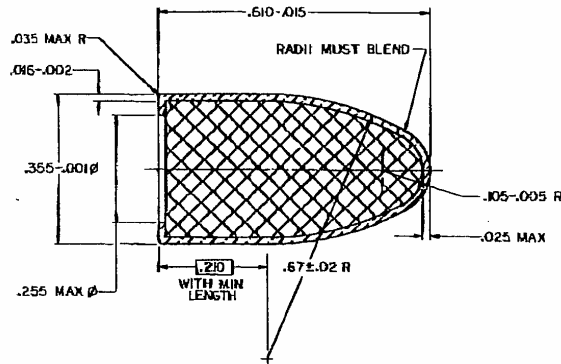


Fig. 3. M882 bullet.

In 2000 tests were performed at the Armed Forces Institute of Pathology (AFIP), in which an M882 was fired at 445 m/s into a multi-ply Kevlar vest worn by human thoracic tissue. The vest was composed of plain-woven, 600-denier Kevlar KM2. The bullet was aimed at the center of the sternum. Endevco accelerometers were surgically implanted at four locations in the thoracic tissue: the posterior sternum (Fig. 4a), the spinous process of the T7 vertebra (Fig. 4b), the carina (bifurcation point) of the trachea, and the ligamentum arteriosum (Mackiewicz, in preparation).

The AFIP tests were simulated using the LS-DYNA FE code (Livermore Software Technology Corp., 2003.) An FE model of the vest was added to the exterior of WSTM using HyperMesh software (Altair Engineering, 2000) (Fig. 5). The vest’s mesh consisted of one 8-node solid (“brick”) element through the thickness. The typical vest element had in-plane edge lengths of about 10 mm (consistent with the typical element size of WSTM) and a 3.63-mm thickness. This thickness is the ratio of the vest’s known areal density and the volumetric density of 1440 kg/m³ that has been used for Kevlar (Johnson, et al., 1999). Isotropic Hooke’s law was applied, with a Young’s modulus of 74 GPa and a Poisson’s ratio of 0.2.

These values were also obtained from Johnson et al. (1999). The M882 bullet was modeled with a single lead element, to which perfect plasticity was applied with an initial density of 11350 kg/m³, an elastic shear modulus of 5.52 GPa, and a flow stress of 34.5 MPa.

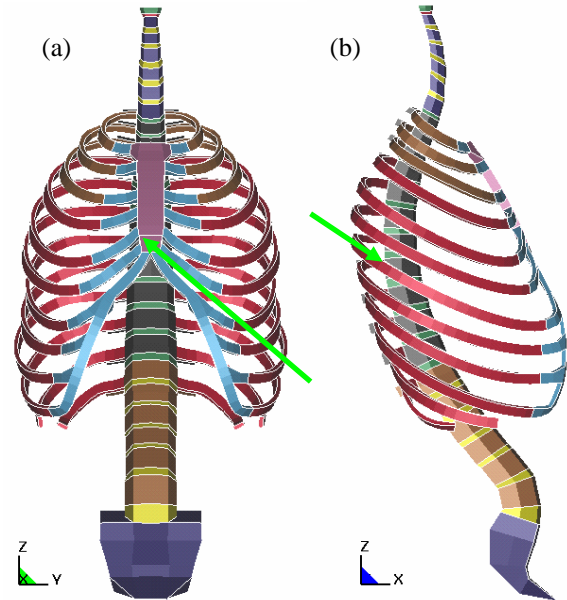


Fig.4. Two accelerometer locations in the AFIP tests: (a) posterior sternum, (b) spinous process of T7 vertebra.

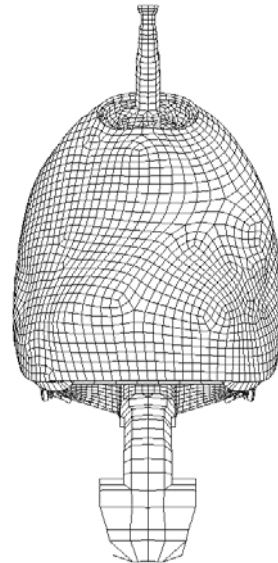


Fig. 5. Kevlar vest added to the WSTM.

Figure 6 compares the LS-DYNA result at the posterior sternum with the measured signal from one of the tests. The accelerometer was an Endevco

7270A-20K, with an amplitude range of 20×10^3 g's and a frequency range of 50 kHz (Endevco Corp., 2001). The FE solution was sampled at 20 μ s intervals to be consistent with the gauge's frequency response. A general agreement between theory and experiment was achieved, although oscillations are observed in the computations that were not present in the experiment. Less capable accelerometers, in terms of both amplitude and frequency response, were employed at the sternum in the other two tests and at the other three locations in all four tests. In general, at the other three locations the FE signal exceeded in amplitude the measured signal. See Raftenberg (2003) for details. Conclusions took the form of recommended improvements to the Kevlar fabric modeling (pursued in section 3) and to the WSTM thorax model (pursued in section 4), and suggested sources of error in the experiments. The latter include slippage of the sutured gauge and inertial loading provided by the gauge.

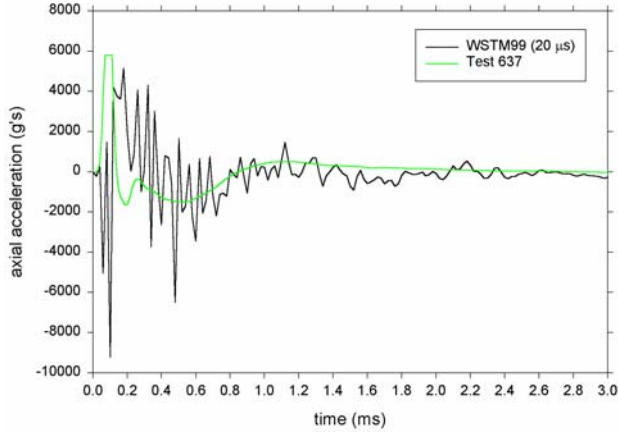


Fig. 6. FE results and AFIP data for sternum acceleration.

3. PROGRESS IN MODELING THE KEVLAR VEST

In section 2 the Kevlar vest was modeled using isotropic linear elasticity. Figure 7 provides a sketch of the plain-weave construction of each ply of the vest. Plain-weave consists of two initially mutually orthogonal families of yarns called *warp* and *fill*, or *weft*. Note the coordinate system defined in the figure. Material coordinates X_1 , X_2 , and X_3 coincide with the warp yarns, fill yarns, and the *transverse* (through-thickness) direction, respectively. Based on this construction, one would expect material orthotropy rather than isotropy to characterize this vest. Figure 8, reproduced from Raftenberg, et al. (in review), presents stress-strain data from a single ply of plain-woven, 600-denier Kevlar KM2 pulled in quasi-static, uniaxial tension along its warp yarns. Figure 9,

reproduced from Raftenberg, Scheidler, and Moy (2004), presents stress-strain data from the multi-ply Kevlar vest subjected to quasi-static, uniaxial, transverse compression. Figures 8 and 9 make clear that the vest's stress-strain response is nonlinear as well as anisotropic. The in-plane tensile nonlinearity in Fig. 8 can be attributed, at least in part, to progressive yarn decrimping. The transverse compressive nonlinearity in Fig. 9 can be at least partly attributed to the progressive squeezing out of air from the vest.

Hence, ARL is engaged in the development of a vest constitutive model that is nonlinear, orthotropic, and hyperelastic. The entire vest is viewed as a homogeneous continuum (Fig. 10). The model is assigned the same initial thickness L_0 as measured on the physical vest using a micrometer, an initial density ρ_0 given by

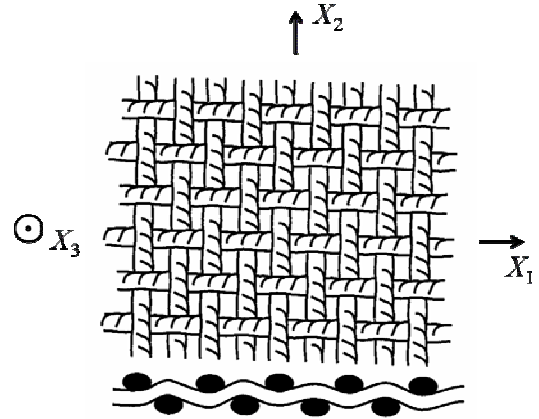


Fig. 7. The plain-weave construction of a single ply, and a Cartesian material coordinate system.

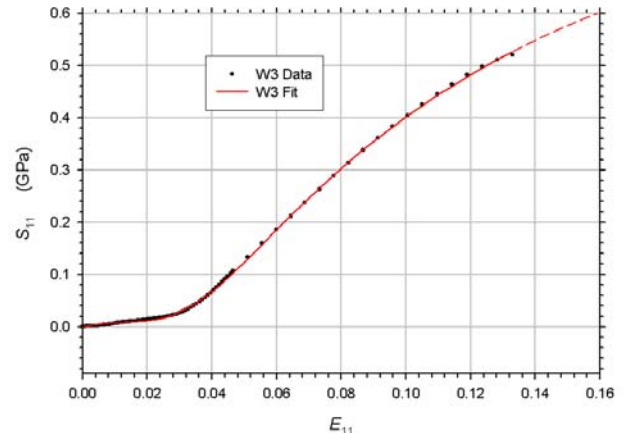


Fig. 8. Second Piola-Kirchhoff stress versus Green strain, both along the warp-yarn direction, for a ply of plain-woven, 600-denier Kevlar KM2 pulled in quasi-static, uniaxial tension along the warp-yarn direction.

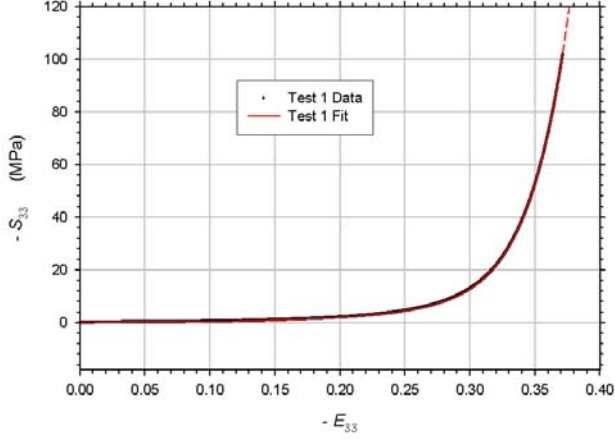


Fig. 9. Second Piola-Kirchhoff stress versus Green strain, both along the transverse direction, for a multi-ply vest composed of plain-woven, 600-denier Kevlar KM2 quasi-statically, uniaxially compressed along the through-thickness (transverse) direction.

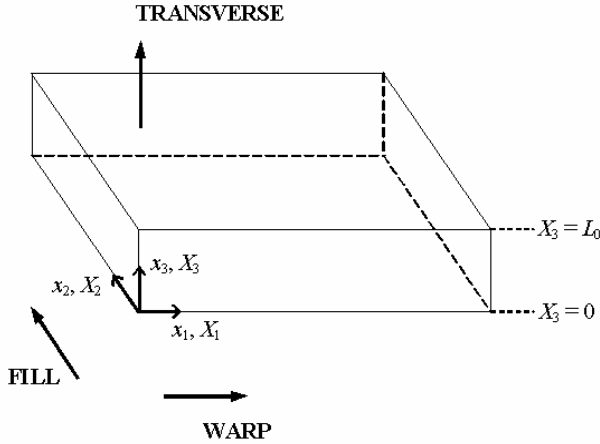


Fig. 10. The vest modeled as a homogeneous, orthotropic continuum.

$$\rho_0 = \frac{\text{vest's areal density}}{L_0}, \quad (1)$$

and we seek a constitutive relation of the form

$$\mathbf{S} = \boldsymbol{\varphi}(\mathbf{E}). \quad (2)$$

Here, \mathbf{E} is the Green strain tensor, \mathbf{S} is the second Piola-Kirchhoff stress tensor, and $\boldsymbol{\varphi}$ is a tensor function. (See Malvern [1969] for definitions of \mathbf{E} and \mathbf{S} .)

Next, motivated by the plain-weave construction in Fig. 7, we introduce the *decoupling* assumption, whereby, each component of \mathbf{S} is a function only of the single corresponding component of \mathbf{E} . More specifically, in terms of the coordinate system defined in Fig. 10,

$$S_{11} = \phi_w(E_{11}) \quad (3a)$$

$$S_{22} = \phi_f(E_{22}) \quad (3b)$$

$$S_{33} = \phi_t(E_{33}) \quad (3c)$$

$$S_{12} = 2G_{wf}E_{12} \quad (3d)$$

$$S_{23} = 2G_tE_{23} \quad (3e)$$

$$S_{31} = 2G_tE_{31}. \quad (3f)$$

This constitutive model introduces two constant shear moduli, G_{wf} and G_t , and three nonlinear functions, ϕ_w , ϕ_f , and ϕ_t . *Warp function*, ϕ_w , and *transverse function*, ϕ_t , are sketched in Figs. 11 and 12, respectively. *Fill function*, ϕ_f , has the same qualitative features as ϕ_w .

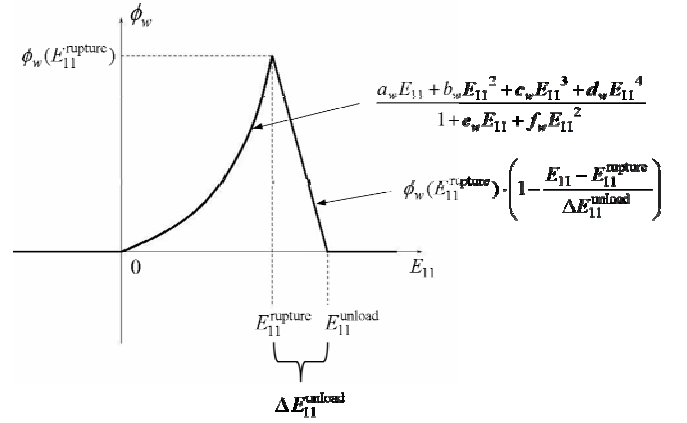


Fig. 11. Warp function, ϕ_w .

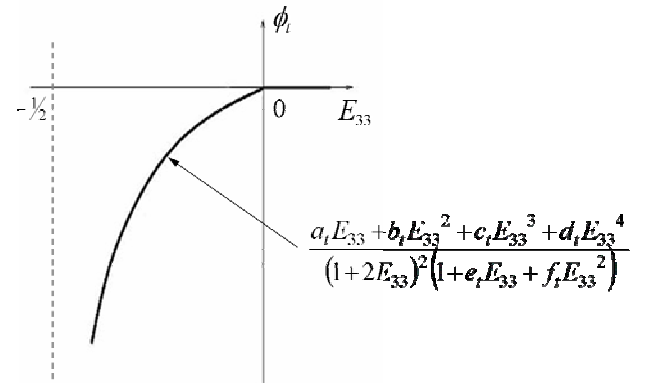


Fig. 12. Transverse function, ϕ_t .

ϕ_w in Fig. 11 can be described in terms of four subdomains: compression ($E_{11} < 0$), tension prior to “rupture” ($0 \leq E_{11} < E_{11}^{\text{rupture}}$), post-rupture tensile unloading ($E_{11}^{\text{rupture}} \leq E_{11} < E_{11}^{\text{rupture}} + \Delta E_{11}^{\text{unload}}$), and completely failed material ($E_{11}^{\text{rupture}} + \Delta E_{11}^{\text{unload}} \leq E_{11}$). The warp yarns are assumed to buckle immediately under axial compression, so that $\phi_w = 0$ throughout the compressive subdomain. For $0 \leq E_{11} < E_{11}^{\text{rupture}}$, ϕ_w consists of a rational function that introduces six material constants: a_w, b_w, c_w, d_w, e_w , and f_w . Mathematica software (Wolfram, 1999) was used to apply nonlinear regression to evaluate these constants. The results, given in Table 1, were found to produce a good fit to the uniaxial tension data throughout this subdomain (Fig. 8). E_{11}^{rupture} , the strain that defines the boundary between the second and third subdomains and that corresponds to the maximum load level reached in the tension test, constitutes the seventh material constant associated with ϕ_w . The value assigned to E_{11}^{rupture} in Table 1 is a direct measurement. For $E_{11} > E_{11}^{\text{rupture}}$, the model assumes a subsequent linear ramping down of stress with increasing strain (Fig. 8). This ramp introduces an eighth material constant, strain increment $\Delta E_{11}^{\text{unload}}$, corresponding to completed specimen unloading, i.e., $\phi_w = 0$ for $E_{11} \geq (E_{11}^{\text{rupture}} + \Delta E_{11}^{\text{unload}})$. $\Delta E_{11}^{\text{unload}}$ may be amenable to direct experimental evaluation, but the value of 0.4 given in Table 1 was chosen to avoid large element distortion in the ballistic simulation.

Fill function ϕ_f describes the stress-strain response in a quasi-static, uniaxial test in which a single-ply specimen is strained along its fill yarns. As was mentioned, ϕ_f was found to be qualitatively similar to the ϕ_w of Fig. 11. ϕ_f introduces the eight analogous material constants $a_f, b_f, c_f, d_f, e_f, f_f, E_{22}^{\text{rupture}}$, and $\Delta E_{22}^{\text{unload}}$. The first six were again evaluated by nonlinear regression performed with Mathematica software. E_{22}^{rupture} was determined directly from the tension test. The value of 0.4 used for $\Delta E_{22}^{\text{unload}}$ was again chosen to avoid large element distortion in the ballistic simulation.

The transverse function ϕ_t in Fig. 12 is divided into two subdomains: compression ($-1/2 < E_{33} \leq 0$) and tension ($0 < E_{33}$). ϕ_t is assumed to be zero in tension because the plies of the Kevlar vest are generally only sparsely stitched together. Note that $-1/2$ is an unattainable lower bound on E_{33} that corresponds to the state of zero thickness. In the allowable compressive

subdomain, ϕ_t is governed by a function introducing six material constants, a_t, b_t, c_t, d_t, e_t , and f_t . This function has a singularity at $E_{33} = -1/2$ to associate infinite stress with infinitesimal thickness. Constants a_t, b_t, c_t, d_t, e_t , and f_t were evaluated by nonlinear regression using Mathematica. The values are added to Table 1, and the resulting fit is seen in Fig. 9 to be good over the entire range of compressive data.

Table 1. Material constants for the multi-ply, 600-denier, Kevlar KM2 vest

a_w (GPa)	1.35322	a_f (GPa)	1.79587
b_w (GPa)	-98.8705	b_f (GPa)	-204.612
c_w (GPa)	2727.95	c_f (GPa)	14539.8
d_w (GPa)	-4898.41	d_f (GPa)	-33428.5
e_w	-22.0527	e_f	-34.3400
f_w	465.297	f_f	2137.94
E_{11}^{rupture}	0.132930	E_{22}^{rupture}	0.149961
$\Delta E_{11}^{\text{unload}}$	0.4	$\Delta E_{22}^{\text{unload}}$	0.4
a_t (MPa)	1.25770	G_{wf} (GPa)	1.0
b_t (MPa)	-7.68533	G_t (GPa)	50.
c_t (MPa)	-71.1591		
d_t (MPa)	-135.116		
e_t	4.74248		
f_t	6.00453		

Equations 6d – 6f relate each shear stress component linearly to its corresponding shear strain component. This introduces the constant elastic shear moduli, G_{wf} and G_t . The former governs in-plane shear, i.e., relative rotation between warp and fill yarns. Currently we have no constitutive data with which to evaluate G_{wf} . We have assigned it the relatively small value of 1.0 GPa in order to incorporate the “scissoring” phenomenon, i.e., reasonably unimpeded in-plane relative rotation of the two families of yarns. Shear modulus G_t was assigned its large value of 50 GPa in order to avoid element collapse in the ballistic simulation.

Finally, the role of the physical vest’s multi-ply construction in reducing the bending stiffness must be considered. According to linear elastic plate theory, a plate’s flexural rigidity, which measures its resistance to bending, increases as the plate’s thickness cubed

(Timoshenko and Woinowsky-Krieger, 1959). Let h be the undeformed thickness of each ply of the physical vest, and let N be the number of plies in the vest. If, in the physical vest, each ply behaves as an independent plate with its own neutral surface, then the net flexural rigidity of the vest is KNh^3 , where K is a constant determined by material properties. On the other hand, if one were to model the entire vest as a single plate with thickness Nh ($=L_0$), the resulting bending stiffness of the model would equal $K(Nh)^3$, in general a much larger quantity than KNh . To mitigate excessive bending stresses, we introduce internal frictionless contact surfaces (“slidelines”) within the vest. In Fig. 13 we show four such slidelines, and the vest is correspondingly modeled with five 8-node brick elements through its thickness.

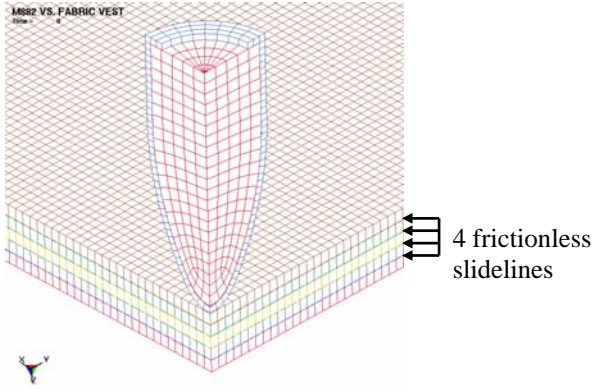


Fig. 13. Finite element models for the vest and the M882 bullet.

In order to benchmark the FE fabric model prior to placing it on a thorax, we applied the model in an LS-DYNA simulation of a ballistic test involving the vest impacted by a M882 at 370 m/s (Raftenberg, Scheidler, and Moynihan, 2004). A Phantom V5 camera was employed to capture silhouettes (2D projections) of the vest’s back face. These stills were then digitized at 60- μ s intervals to obtain back-face deflection data (Fig. 14). In the test the bullet arrested and began to recoil at 680 μ s after impact. At that time, the vest’s back-face displacement at the point directly beneath the bullet had attained a value of about 52 mm.

In the LS-DYNA simulation the M882 bullet was approximated by a cylindrical disc of lead having an initial diameter, D_0 , equal to the final diameter of the bullet recovered after the test (Fig. 15). The disc’s initial height, h_0 , was chosen to according to the relation

$$\frac{\pi}{4} \rho_{\text{lead}} D_0^2 h_0 = 8 \text{ grams} \quad , \quad (4)$$

where ρ_{lead} is the undeformed density of lead.

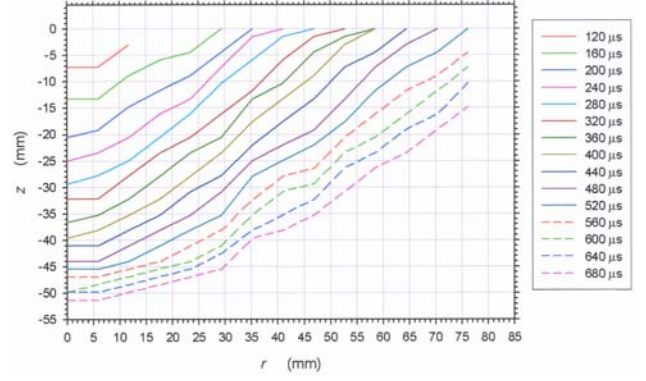


Fig. 14. Measured back-face deflection of the vest following impact by an M882 bullet at 370 m/s.

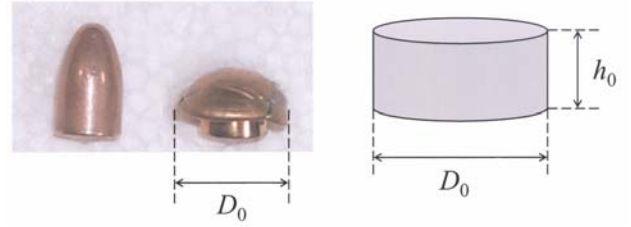


Fig. 15. The M882 bullet was approximated by a disc.

By 70 μ s after impact, the time step in the LS-DYNA simulation, determined from the Courant stability condition, had effectively diminished to zero. The solution up to that time is compared with experiment in Fig. 16. Near agreement with experiment was achieved in the rate of radial spread of the displacement field. I.e., the radial distance traveled by the Z-displacement wave during the 40 μ s interval between 120 and 160 μ s in the experiment is about equal to the computed radial distance traveled during the 30 μ s interval between 30 and 60 μ s. However, there are two notable points of disagreement between theory and experiment. First is the time required for initial appreciable back-face displacement, which was between 80 and 120 μ s after initial impact in the test and between 10 and 20 μ s in the computations. The second point of disagreement is in the magnitude of the back-face displacement. While the peak magnitude in the test was about 52 mm (Fig. 14), at 70 μ s a magnitude of only 11 mm was attained in the computations. The bullet in the computations was still moving at 70 μ s, but its center-of-mass velocity had diminished by about 78%, from its initial value of 370 to about 80 m/s (Fig. 17). Hence it is unlikely that a displacement of 52 mm would eventually be attained.

The conclusion is that the FE fabric model is too stiff. Possible sources of the excess stiffness include the neglect of rate effects, the neglect of multi-axial coupling, and

failed in that spurious penetration of internal contact surfaces occurred.

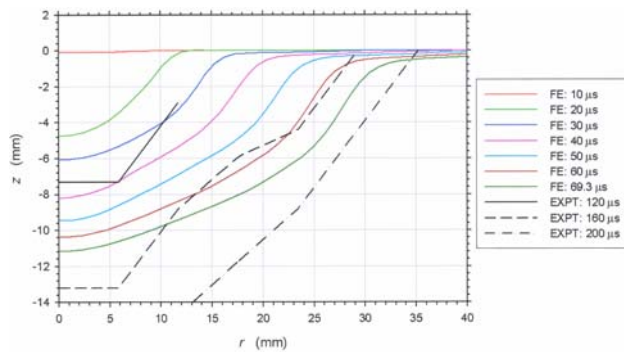


Fig. 16 The vest's back-face deflection following impact by an M82 bullet at 370 m/s; LS-DYNA results compared with experiment.

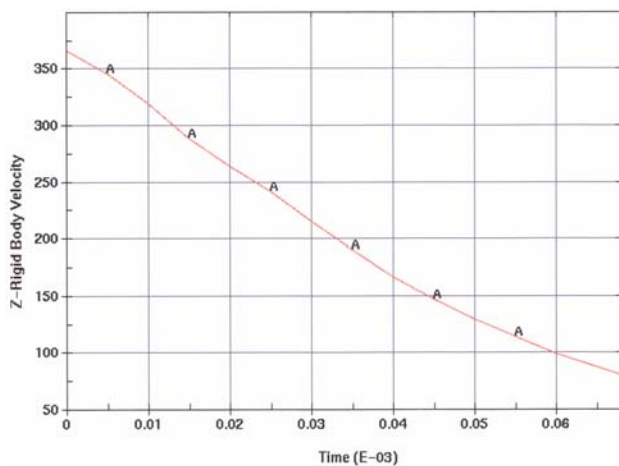


Fig. 17. The computed center-of-mass velocity of the lead disc versus time.

4. A COMPUTATIONALLY ROBUST THORAX MODEL

The WSTM, with its extensive anatomical detail, contains numerous internal contact surfaces (slidelines) between adjacent parts. The model functioned to produce plausible results for the ballistic application of section 2, involving impact by an M882 at 445 m/s.

However, a second situation of great interest is the NIJ Level III design threat, namely an M80 bullet impacting at 823 m/s. The M80 is a NATO round with a 7.62 mm diameter, also composed of a lead core and a gilding jacket (Fig. 18). When WSTM was applied to this more energetic impact, the LS-DYNA contact algorithm

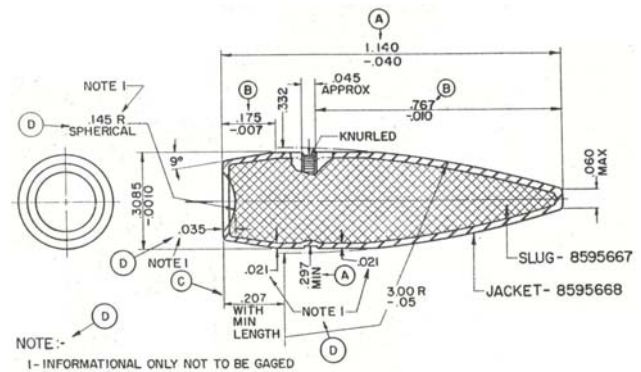


Fig. 18. M80 7.62-mm NATO round.

To address this challenge, we are currently developing an FE thorax model that is simpler than WSTM. The aim is to discard parts of secondary structural importance and thereby create a more robust model having fewer contact surfaces.

The revised thorax model is divided into internal parts (Fig. 19) and an external casing (Fig. 20). The internal parts preserve WSTM's representation of the circulatory and respiratory systems. However, these parts are now more finely meshed, with a typical edge length of 5 mm, reduced from 10 mm in WSTM.

The external casing consists of the spinal column, the diaphragm forming the “floor” of the thoracic cavity, and an enclosing shell part that represents the ribs and the muscles lining the ribcage.

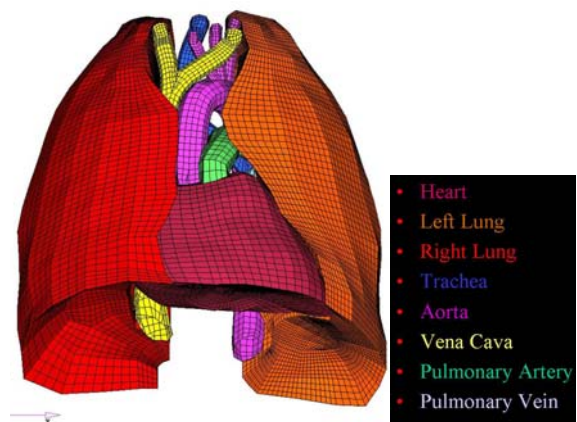


Fig. 19. Internal parts of the thorax model.

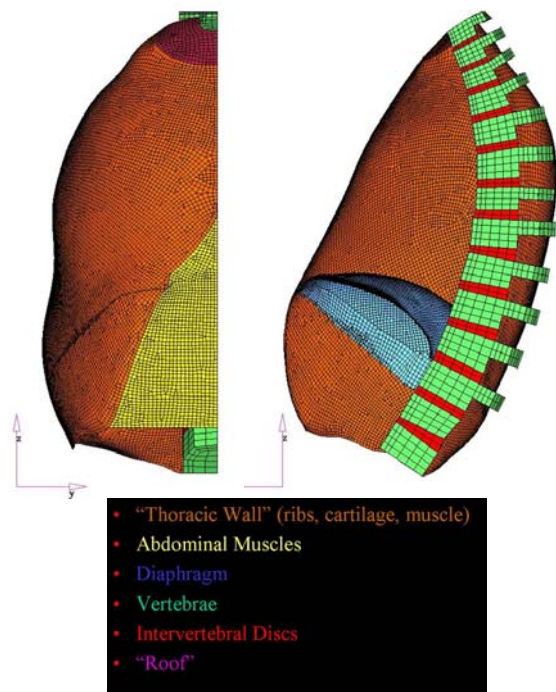


Fig. 20. The outer casing of the thorax model.

CONCLUSIONS

ARL is striving to develop an FE-based design capability for thoracic body armor. Towards this end, progress has been made in developing FE models for Kevlar vests and for the human thorax.

Future plans regarding the fabric model include numerical experimentation to determine the required number of internal slidelines. We are also seeking to expand the experimental database to include multi-axial loading and high-rate loading. Such new data would allow us to examine our current assumptions of decoupling and rate independence.

Future plans regarding the thorax model include the addition of internal fluid to represent the structural contributions of cells. In addition we plan to revise the constitutive modeling of various biomaterials to incorporate recent advances in the experimental database.

ACKNOWLEDGMENTS

The fabric model of section 3 was a collaborative effort. Dr. Michael J. Scheidler of ARL contributed substantially to the theoretical development. Paul Moy of ARL provided the data in Fig. 9. Thomas J. Moynihan of DSI Corp. provided the data in Figs. 8 and 14.

REFERENCES

- Altair Engineering, 2000: HyperMesh Tutorials, Version 3.1.
- Endevco Corp., 2001: <<http://www.endevco.com>>.
- Johnson, G.R., Beissel, S.E., and Cunniff, P.M., 1999: A Computational Model for Fabrics Subjected to Ballistic Impact. *Proc. 18th Intl. Symp. Ballistics*, vol. 2, 962-969.
- Livermore Software Technology Corp., 2003: *LS-DYNA Keyword User's Manual*, Version 970, Livermore, CA.
- Mackiewicz, J., Blethen, W., Carlson, T., Prifti, J.J., De Maio, M., Parks, S., Schilke, P., Campman, S., Meyers, C., Georgia, J., and Flemming, D., in preparation: *Effects of Ballistically Induced Blunt Trauma and Correlations to Laboratory Measurement Techniques*, ATC-8444, U.S. Army Aberdeen Test Center, APG, MD.
- Malvern, L. E., 1969: *Introduction to the Mechanics of a Continuous Medium*, Prentice-Hall, Englewood Cliffs, NJ, 154-161, 220-223.
- National Institute of Justice, 1987: *Ballistic Resistance of Police Body Armor*, NIJ Standard 1010.3, U.S. Department of Justice.
- Raftenberg, M. N., 2003: *Response of the Wayne State Thorax Model with Fabric Vest a 9-mm Bullet*, ARL-TR-2897, U.S. Army Research Laboratory, APG, MD.
- Raftenberg, M. N., Scheidler, M. J., and Moy, P., 2004: *Transverse Compression Response of a Multi-Ply Kevlar Vest*, ARL-TR-3343, U.S. Army Research Laboratory, APG, MD.
- Raftenberg, M. N., Scheidler, M. J., and Moynihan, T. J., 2004: *Proceedings from the Personal Armour Systems Symposium 2004*, editor: J. van Bree, The Hague, 6-10 Sept. 2004, 291-302.
- Raftenberg, M. N., Scheidler, M. J., Moynihan, T. J. and Smith, C., in review: *Plain-Woven, 600-Densier Kevlar KM2 Fabric Under Quasi-static, Uniaxial Tension*, ARL-TR, U.S. Army Research Laboratory, APG, MD.
- Timoshenko, S., and Woinowsky-Krieger, S., 1959: *Theory of Plates and Shells*, Second Edition, McGraw-Hill, New York, 3-4.
- Wang, H.-C. K., 1995: *Development of a Side Impact Finite Element Thorax Model*, Ph.D. Thesis, Wayne State University, Detroit.
- Wolfram, S., 1999: *The Mathematica Book*, Fourth Edition, Cambridge University Press.



Modeling Thoracic Blunt Trauma; Towards a Finite-Element (FE)-Based Design Methodology for Body Armor

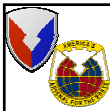
Martin N. Raftenberg

U.S. Army Research Laboratory
Weapons & Materials Research Directorate
Aberdeen Proving Ground, MD 21005-5069

mnr@arl.army.mil

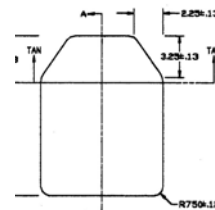
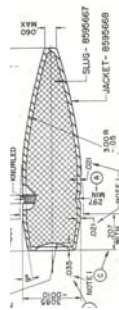
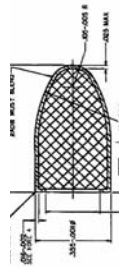
1-410-306-0949

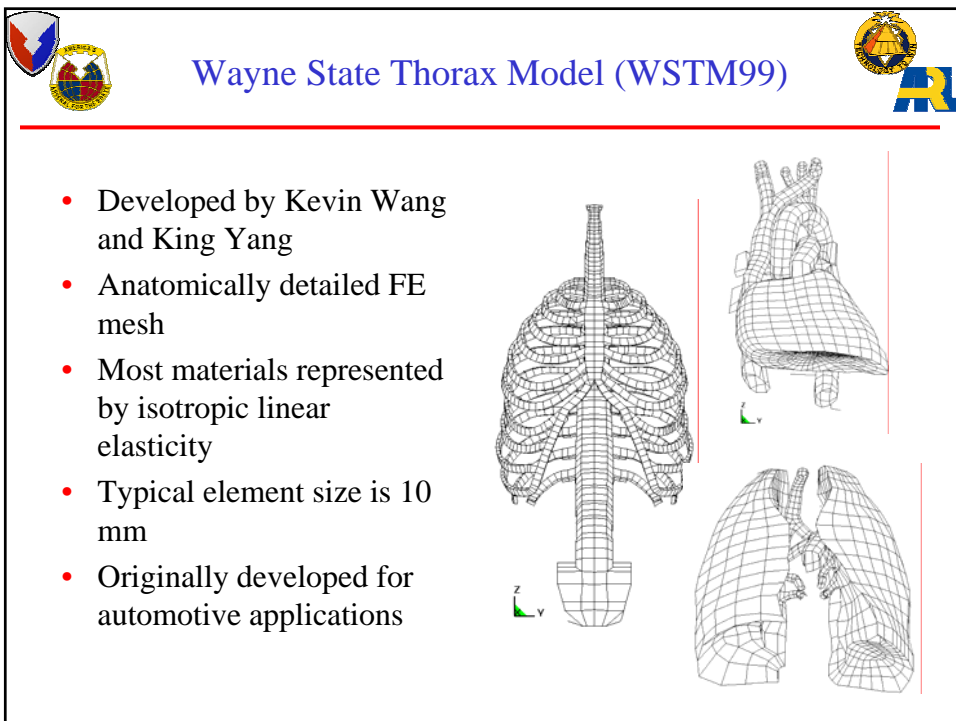
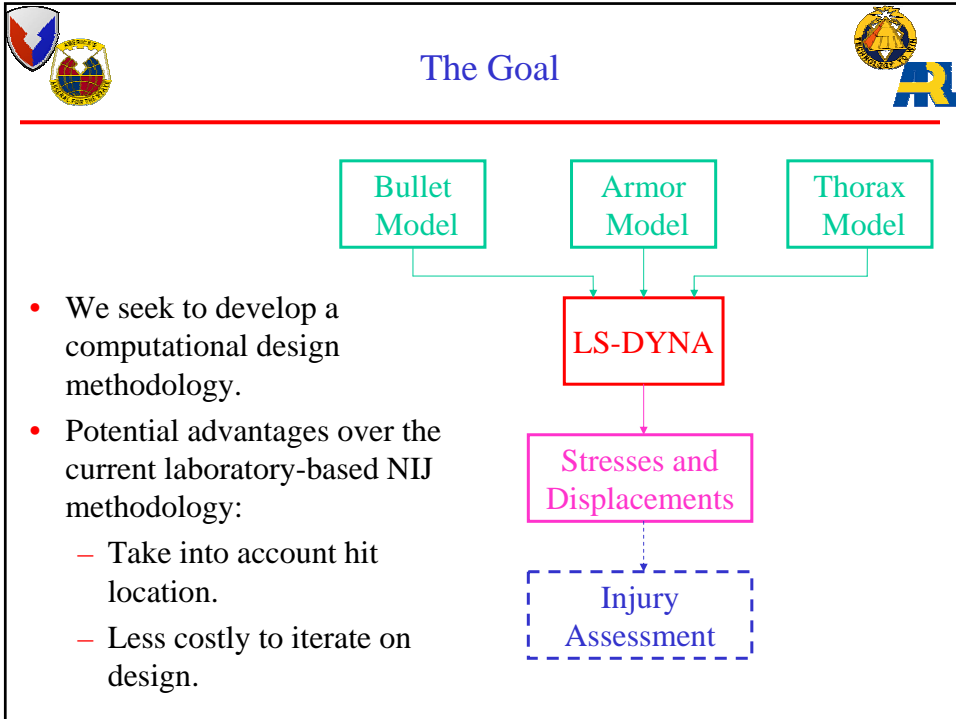
ASC 2004, Orlando, 29 Nov - 2 Dec 2004



NIJ Standard; Levels 3A and 3 Body Armor

- NIJ Level 3A Armor
 - Design Threat: M882 @ 425 m/s
 - Acceptance Criterion: 44-mm Indentation in Plastilina Clay
 - Usual Solution: Kevlar Vest
- NIJ Level 3 Armor
 - Design Threat: M80 @ 823 m/s
 - Acceptance Criterion: 44-mm Indentation into Plastilina Clay
 - Usual Solution: Kevlar Vest + SAPI Plate







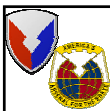
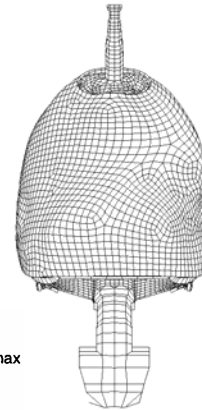
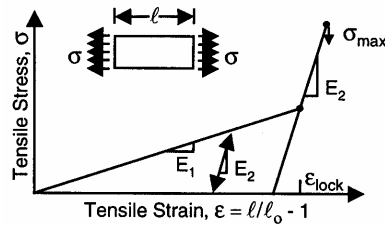
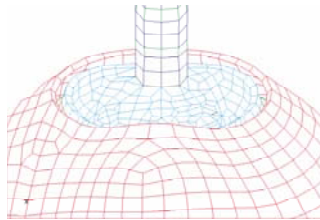
Putting a Vest on WSTM99



- 10-mm in-plane element dimension compatible with WSTM99
- 3.6-mm initial thickness computed using

$$\text{thickness} = \frac{\text{vest's areal density}}{\text{Kevlar's volumetric density}}$$

- Isotropic Hooke's law using Kevlar KM2 data from Johnson, Beissel & Cunniff (1999).

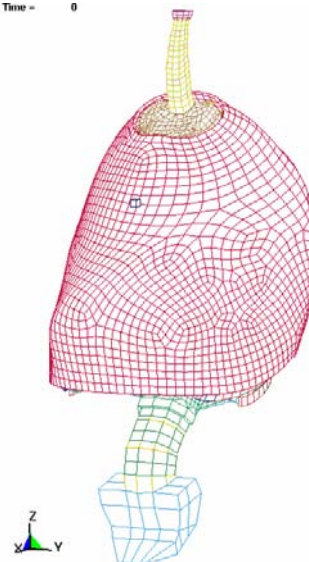


LS-DYNA Simulation: M882 vs. Kevlar Vest + WSTM99



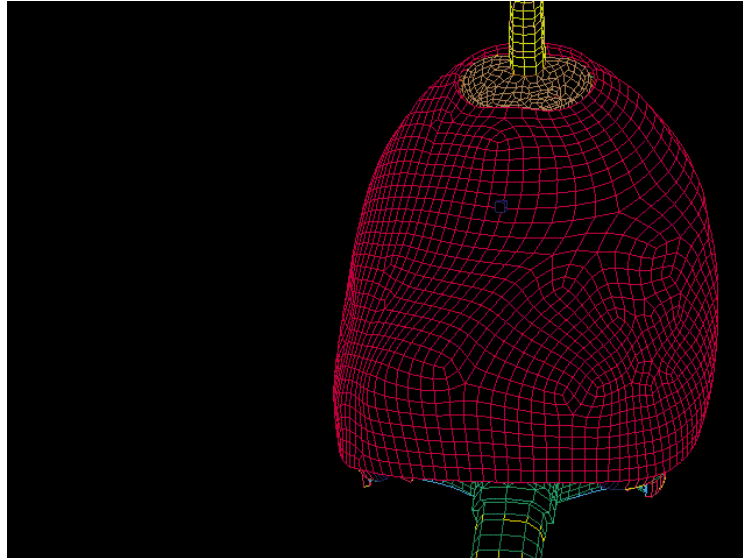
- Bullet modeled with 1 element and Johnson-Cook properties for lead.
- Acceleration results were compared with data from AFIP cadaver tests.
- Some agreement at the sternum; elsewhere computed accelerations exceeded measurements.
- Conclusions involved recommended instrumentation and refinements to WSTM99 and to fabric modeling.
- Documentation:
Raftenberg, ARL-TR-2897, Jan 2003.

Time = 0

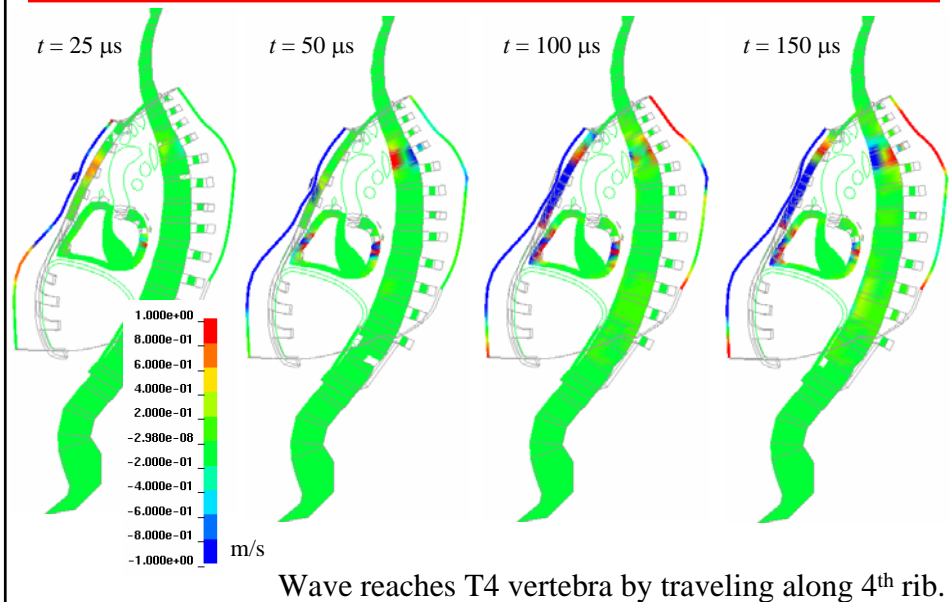


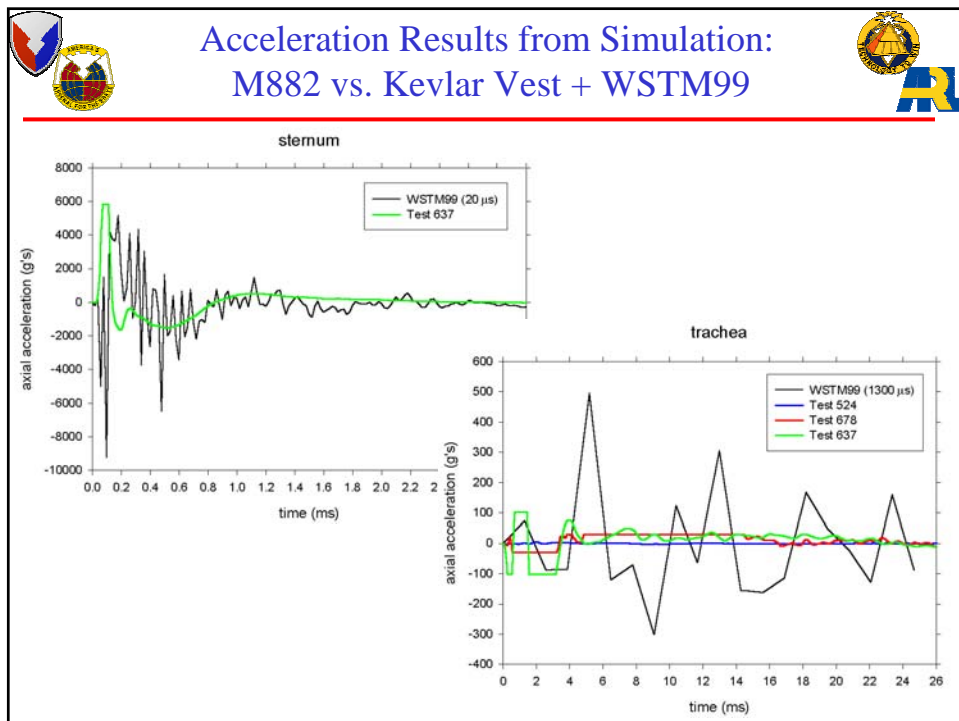
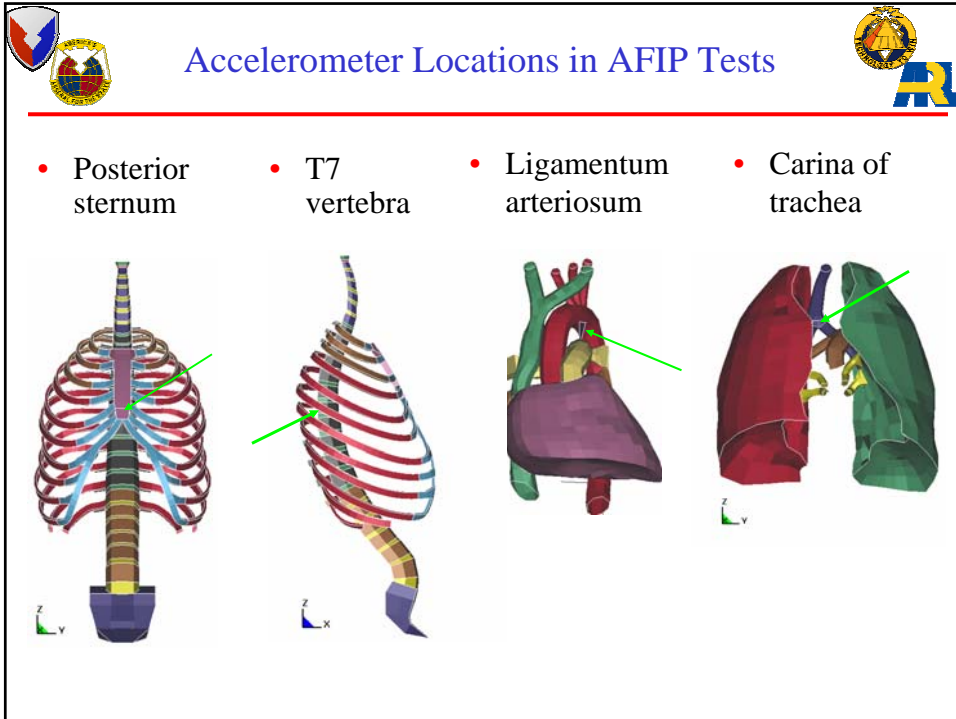


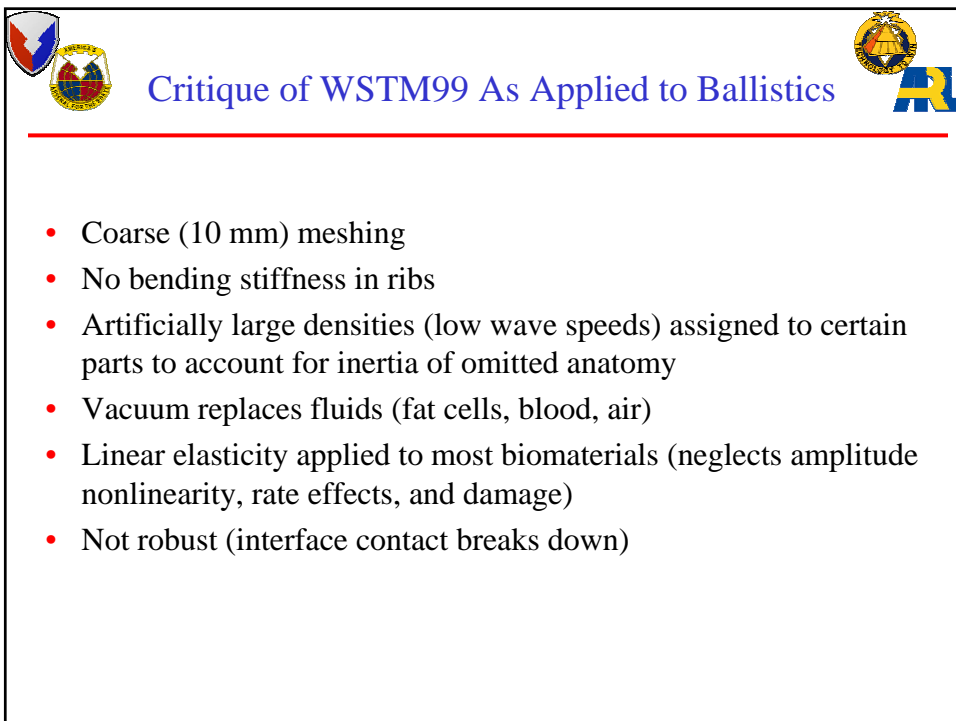
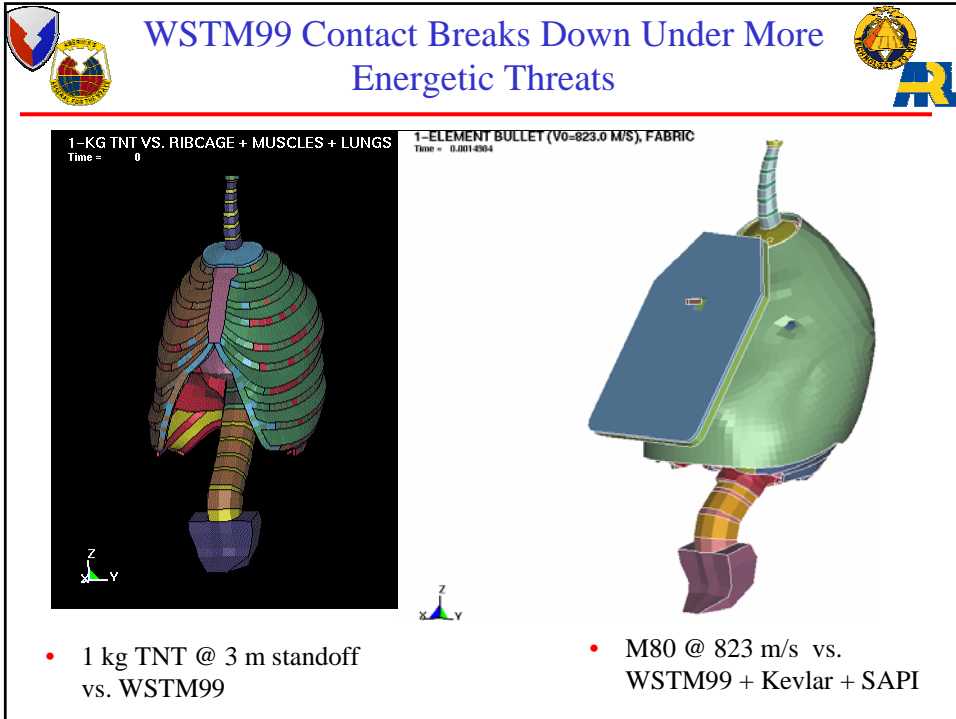
M882 vs. Kevlar Vest + WSTM99



Velocity Results from LS-DYNA Simulation: M882 vs. Kevlar Vest + WSTM99









Suggested Simplifications/Improvements to the WSTM



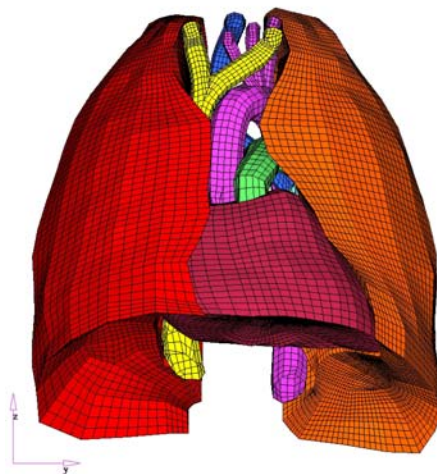
- Two criteria for what to keep:
 - If you don't keep it, you won't get output for it.
 - Heart
 - Lungs
 - Liver

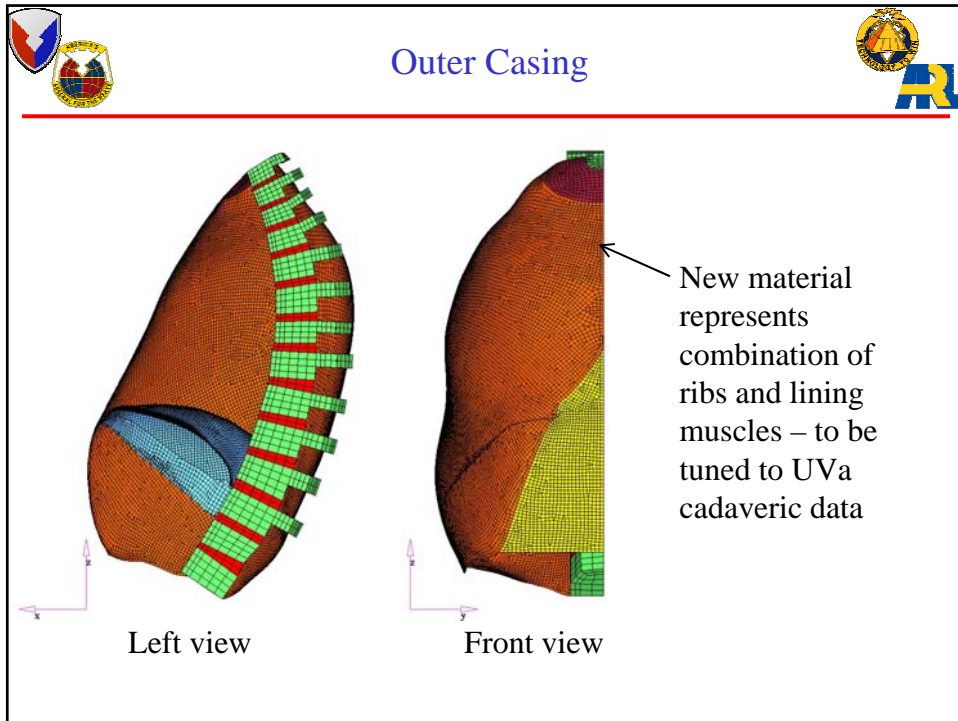
} *sites of "not immediately survivable" injuries*
 - Does its presence affect the solution for the parts of interest?
 - Associated Plumbing – *anchor the Heart & Lungs*
 - Fat, Blood & Air – *transmit load to Heart & Lungs*
 - Ribcage and the Muscles that line it – *main load-bearing elements*
 - Diaphragm
 - Spine


} *seal thoracic cavity*




Internal Parts Remeshed with 5-mm Elements





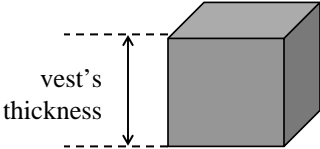


Refined FE Model Development for a Fabric Vest



ARL co-workers:
 Theoretical/computational: Michael Scheidler
 Experimental: Thomas Moynihan, Thomas Mulkern, Paul Moy

- We seek a constitutive model for the vest that is useable in large-scale ballistics calculations involving a bullet, a vest, and a human torso.
- In the interest of computational efficiency, we would prefer that the fabric vest be represented as a homogeneous continuum.



vest's thickness

$$\rho_0 = \frac{\text{vest's areal density}}{\text{vest's initial thickness}}$$

$$\mathbf{S} = \boldsymbol{\varphi}(\mathbf{E})$$



3D Fabric Model



- Decoupled Orthotropic Hyperelasticity

$$S_{ww} = \phi_w(E_{ww})$$

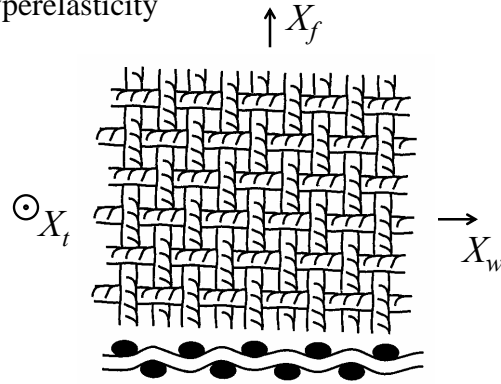
$$S_{ff} = \phi_f(E_{ff})$$

$$S_{tt} = \phi_t(E_{tt})$$

$$S_{wf} = 2G_{wf}E_{wf}$$

$$S_{wt} = 2G_tE_{wt}$$

$$S_{ft} = 2G_tE_{ft}$$

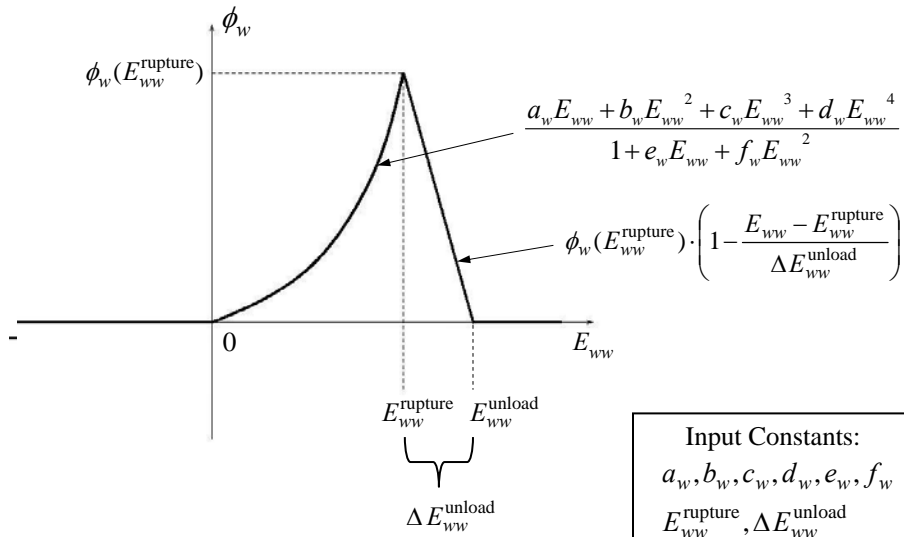


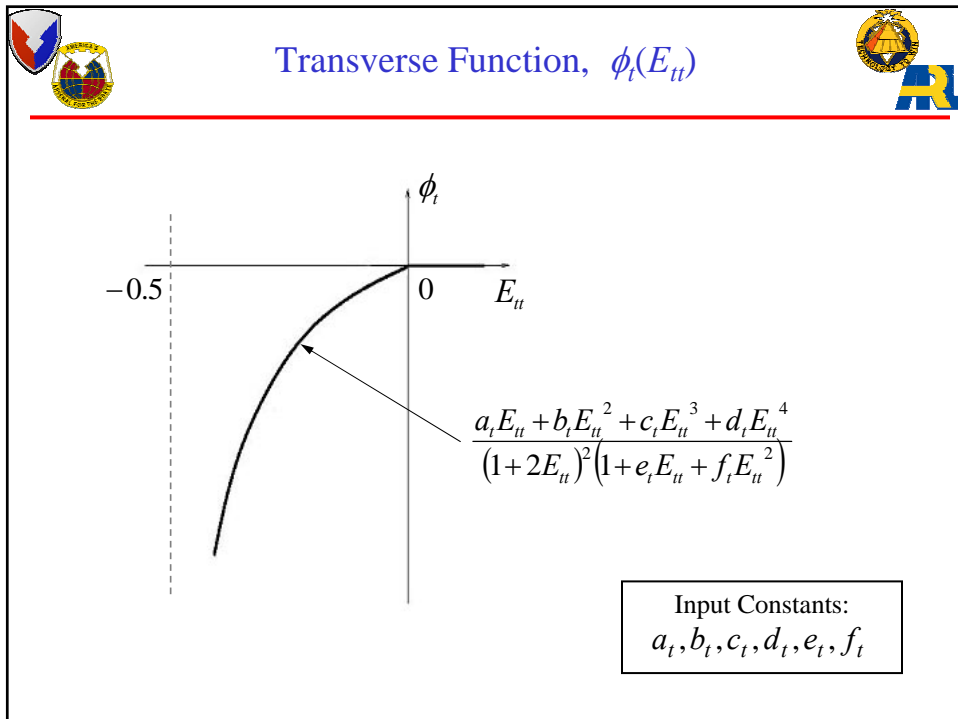
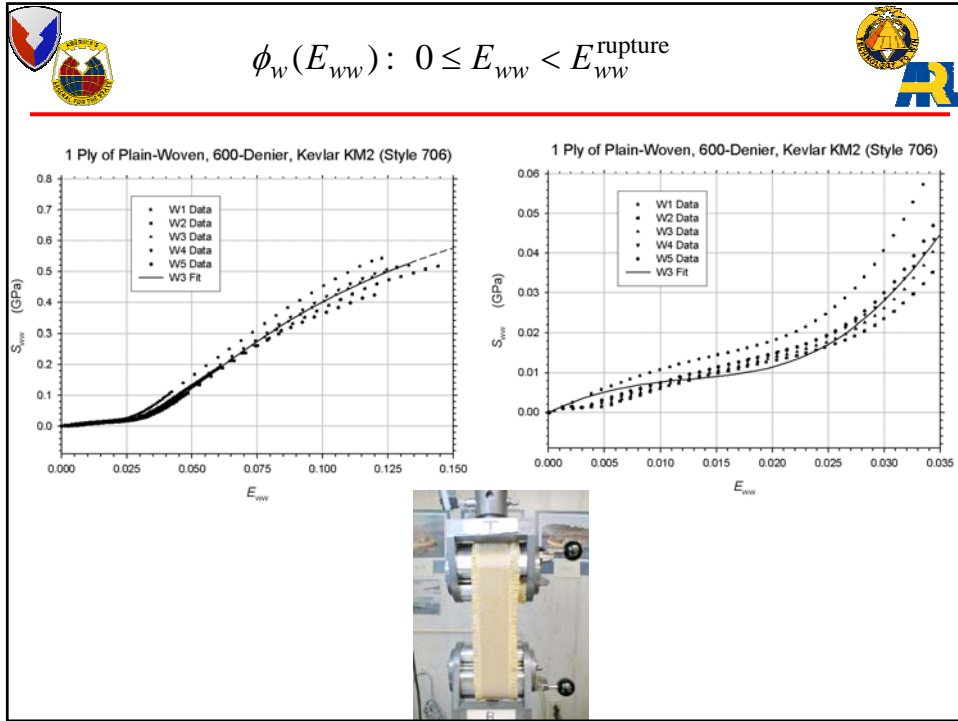
- Introduces the three scalar functions ϕ_w, ϕ_f, ϕ_t .

$$\left[\text{Note that } W(\mathbf{E}) = \int_0^{E_{ww}} \phi_w dE_{ww} + \int_0^{E_{ff}} \phi_f dE_{ff} + \int_0^{E_{tt}} \phi_t dE_{tt} + G_{wf}E_{wf}^2 + G_t(E_{wt}^2 + E_{ft}^2) \right]$$



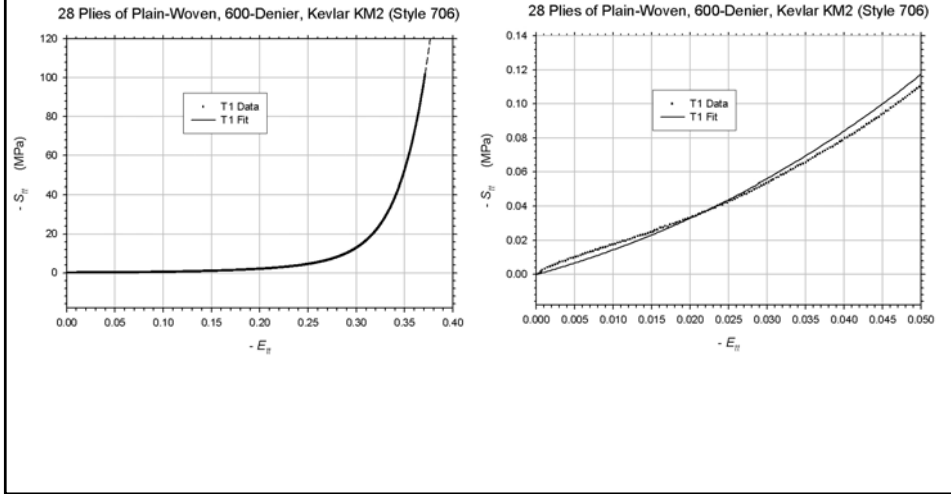
Warp Function, $\phi_w(E_{ww})$







$$\phi_t(E_{tt}): -0.5 < E_{tt} \leq 0$$



Material Constants



a_w (GPa)	1.35322
b_w (GPa)	-98.8705
c_w (GPa)	2727.95
d_w (GPa)	-4898.41
e_w	-22.0527
f_w	465.297
$E_{ww}^{rupture}$	0.132930

a_f (GPa)	1.79587
b_f (GPa)	-204.612
c_f (GPa)	14539.8
d_f (GPa)	-33428.5
e_f	-34.3400
f_f	2137.94
$E_{ff}^{rupture}$	0.149961

a_t (MPa)	1.25770
b_t (MPa)	-7.68533
c_t (MPa)	-71.1591
d_t (MPa)	-135.116
e_t	4.74248
f_t	6.00453

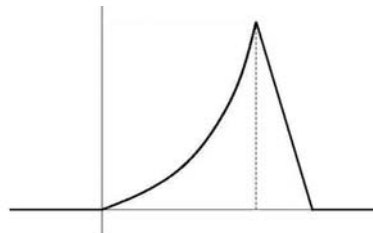
G_{wf} (GPa)	1.0
G_t (GPa)	50.



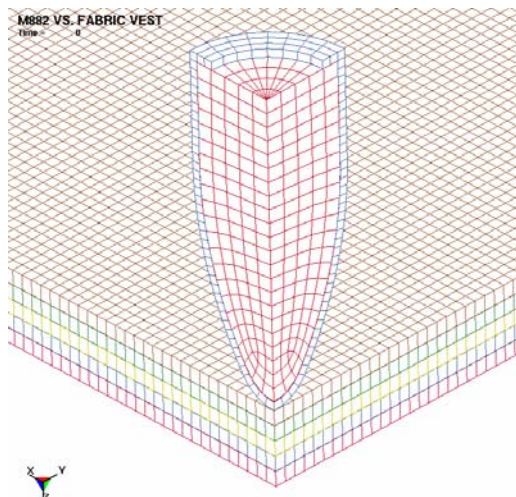
Element Damage and Erosion Criterion



- Applied individually to each non-eroded fabric element at each time step:
 - If $E_{ww} \geq E_{ww}^{\text{rupture}} + \Delta E_{ww}^{\text{unload}}$
thereafter the element can no longer support S_{ww} .
 - If $E_{ff} \geq E_{ff}^{\text{rupture}} + \Delta E_{ff}^{\text{unload}}$
thereafter the element can no longer support S_{ff} .
 - If both conditions have been met, the element is eroded from the mesh.



A Meshing Consideration: Mitigation of Bending Stresses



h = ply thickness

Bending stiffness of vest
with N plies $\propto Nh^3$

Bending stiffness of a
single-ply vest with the
thickness $Nh \propto (Nh)^3$

4 frictionless slidelines



Multi-axial Effects?



- Quasi-static multi-axial testing is needed to check the decoupling assumption.
 - Biaxial in-plane tension tests have been performed on other fabrics.
 - Tri-axial tests (superimposed transverse compression) have not yet been done.



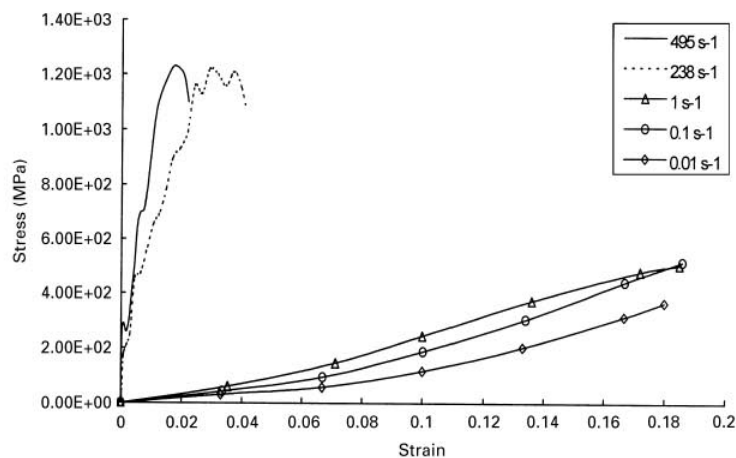
From Boisse et al, NSF Workshop on Composite Sheet Forming, Sept. 5-7, 2001.



Rate Effects?



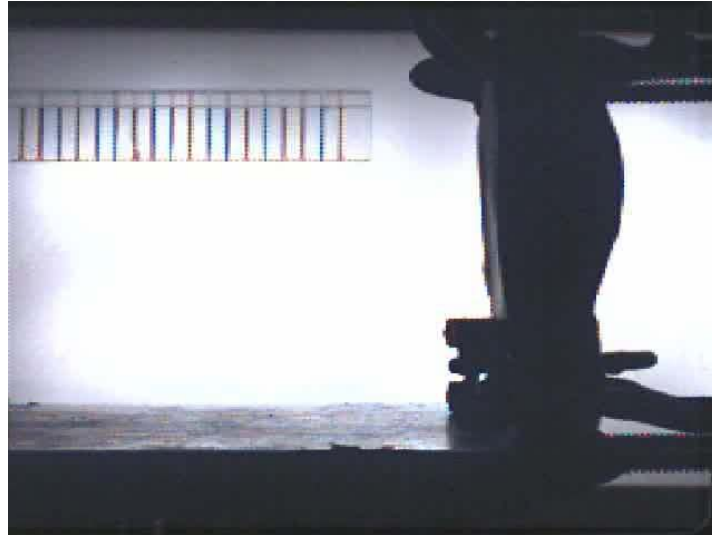
- Extension of the Split Hopkinson Bar technique to woven fabric



Stress-strain data from split Hopkinson bar tests on plain-woven Twaron CT 716 under uniaxial tension. [From Shim, Lim, & Foo. *Int. J. Impact Engrg.*, 25, 2001.]



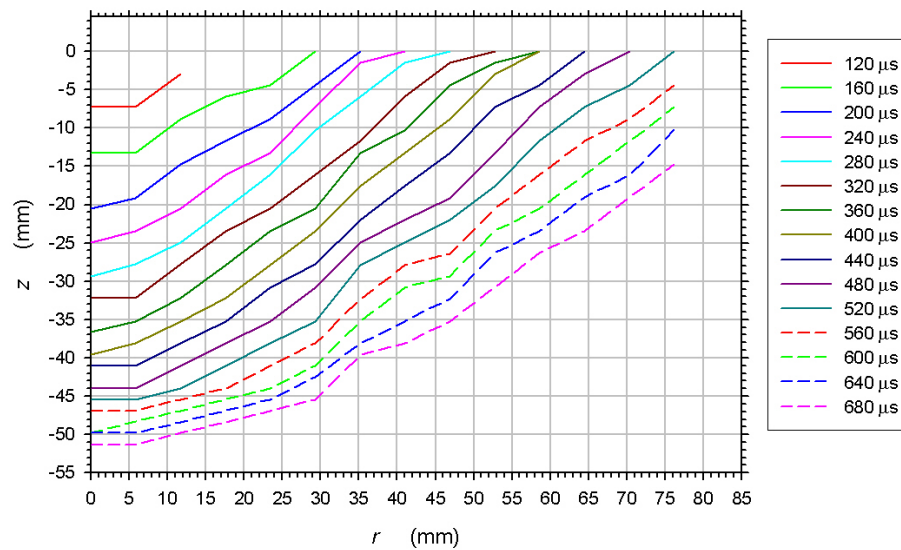
Backface Deflection: M882 @ 380 m/s vs. Fabric Vest



• Visual Solutions V-5 Camera

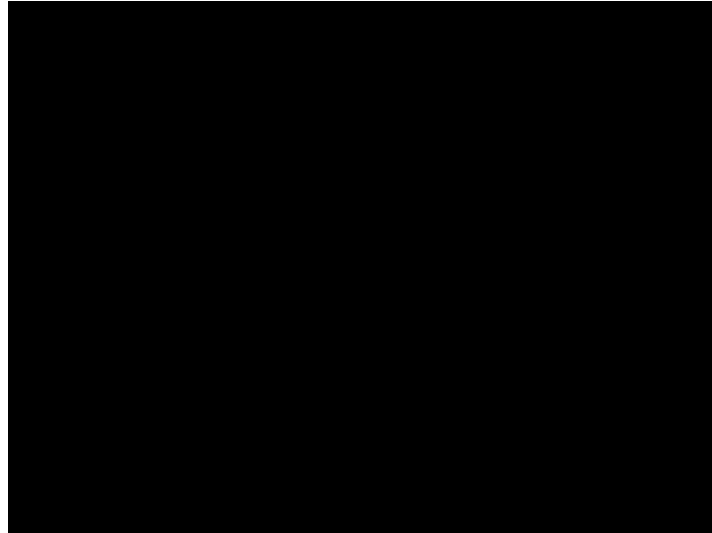


Backface Deflection Data From the Movie (M882 @ 370 m/s vs. Fabric Vest)

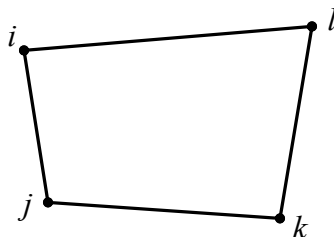




M882 Bullet @ 370 m/s vs. Vest



FE Shape Function Suppresses Mushrooming



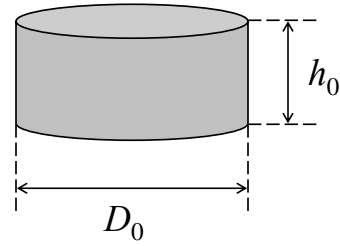
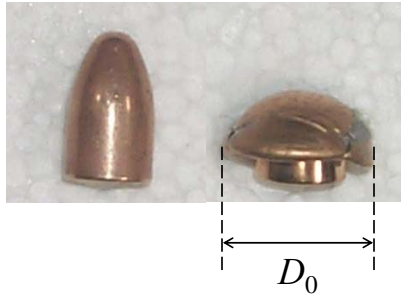
$$v_x(x, y) = a_x + b_x x + c_x y + d_x xy$$

$$v_y(x, y) = a_y + b_y x + c_y y + d_y xy$$

- As the element stretches over a large region, its low-order interpolation functions introduce spurious stiffening.
- Three standard approaches to rectify this
 - Automatic remeshing
 - Particle methods such as SPH
 - Lagrangian-Eulerian hybrid such as ALE



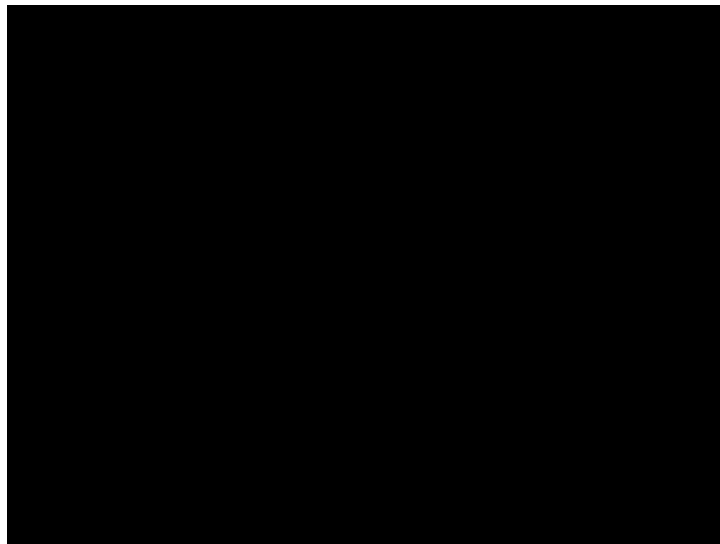
Pre-Mushrooming the Bullet

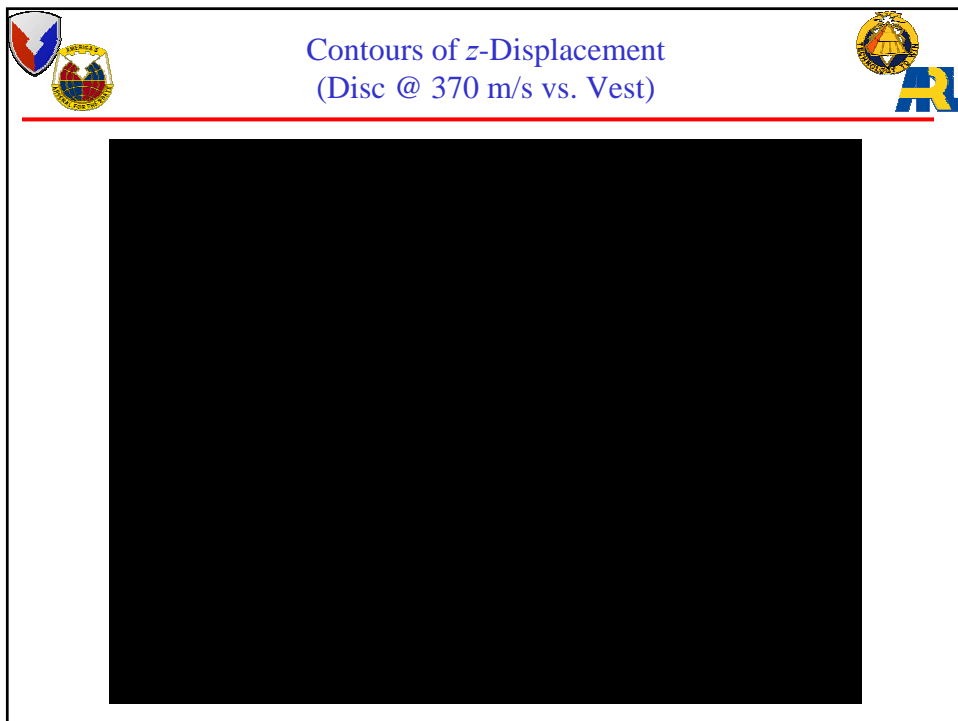
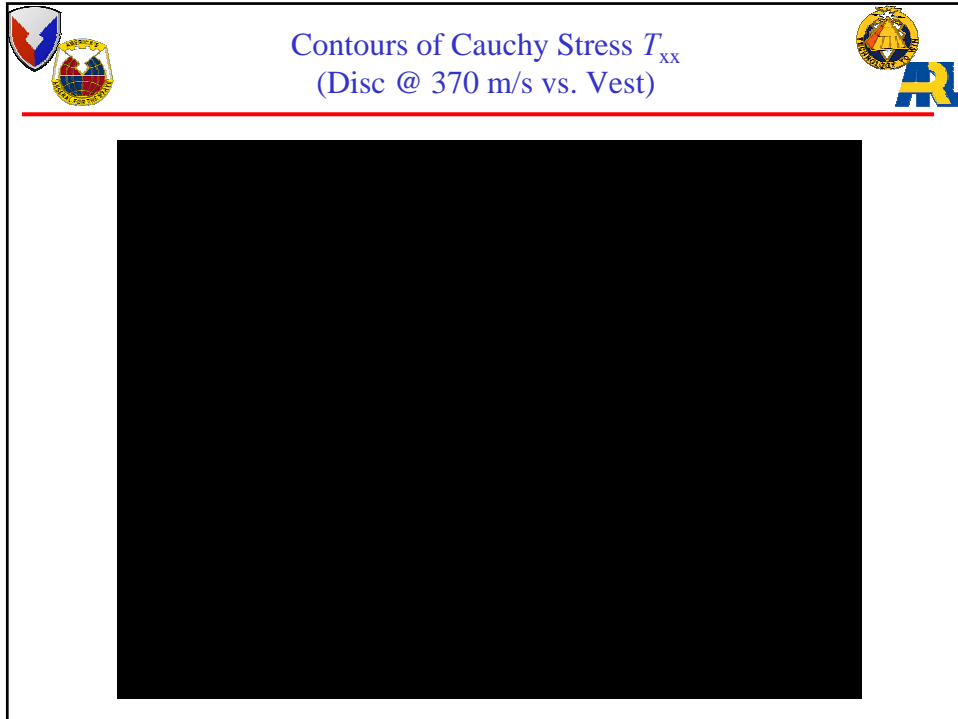


$$\frac{\pi D_0^2 h_0 \rho_{\text{lead}}}{4} = 8 \text{ grams}$$



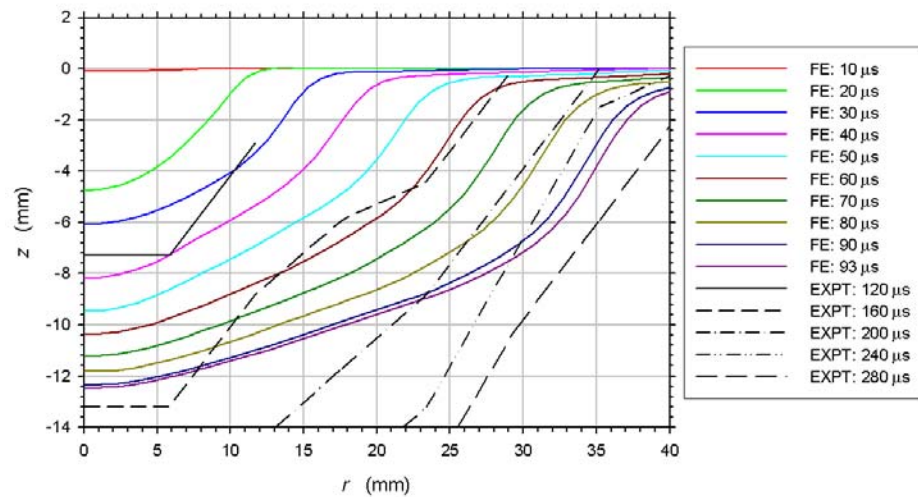
Disc @ 370 m/s vs. Vest



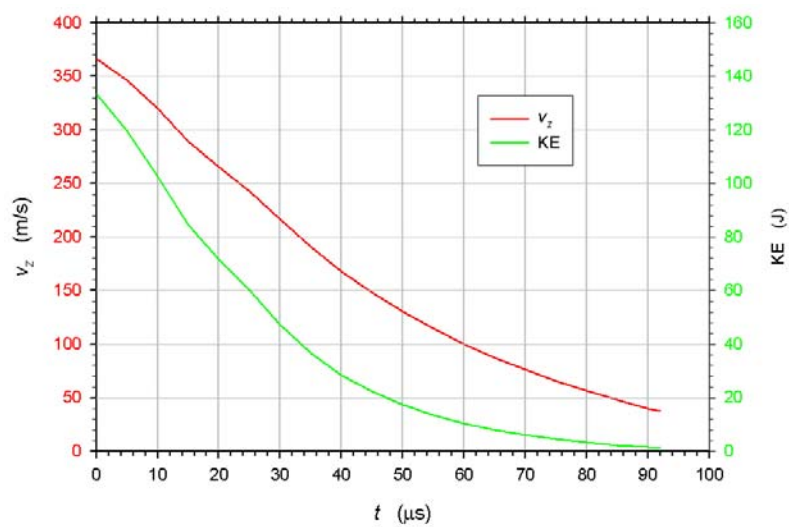




Backface Deflection: FE and Experimental Results (Disc @ 370 m/s vs. Vest)



KE & Center-of-Mass z-Velocity of FE Disc vs. Time





Fabric Modeling: Error Analysis/Planned Improvements



- Features of the Material Model
 - No rate effects
 - No multi-axial coupling effects
- } Awaits
new data
- Features of the FE Application
 - Pre-mushrooming the bullet (plastic work, the bullet's early-time shape) – SPH or ALE should work
 - Spurious bending stiffness if not enough slidelines – numerical experiments will study this
 - Lateral dimensions of target must be increased